Chem Rev Lett 8 (2025) 39-51

Research Article

Chemical Review and Letters
journal homepage: www.chemrevlett.com
ISSN (online): 2645-4947 (print) 2676-7279

Machine Learning-Driven Characterization of Optical Materials: Predicting JO Parameters in Rare-Earth Doped Glasses

Juginder Pal Singh[1], Abdullah Al Hossain Newaz[2], Makarand B Shirke[3], Paul Marcelo Tacle Humanante[4], Man Djun Lee[5] ,Vivek Kumar Pandey[6]

[1]*Dept. of Computer Engineering and Applications, GLA UNIVERSITY, MATHURA-281406, INDIA*
[2]*Masters of Science on Mechanical Engineering, University of Bridgeport, USA*
[3]*Department of Mechanical Engineering , Amrutvahini College of Engineering, Sangamner Maharashtra, India.*
[4]*Facultad de Recursos Naturales, Escuela Superior Politécnica de Chimborazo (ESPOCH), Panamericana Sur km. 1½, Riobamba, 060155, Ecuador.*
[5]*Centre of Mechanical Engineering, Universiti Teknologi Mara (UiTM) Cawangan Johor Kampus Pasir Gudang, Masai 81750, Malaysia*
[6]*Centre for Research Impact & Outcome, Chitkara University Institute of Engineering and Technology, Chitkara University, Rajpura, 140401, Punjab, India*

ARTICLE INFO

Article history:
Received 13 November 2024
Received in revised form 19 December 2024
Accepted 24 December 2024
Available online 25 December, 2024

Keywords:
Organosulfur compounds sulfinic ester
sulfenylating agents
thioethers
carbon-sulfur bond

ABSTRACT

This paper presents a machine learning-driven approach for predicting the spectroscopic properties of rare-earth (RE) doped glass systems, with a focus on Dy^{3+} ions. Glass compositions of 0.25 PbO–0.2 SiO_2–(0.55−x) B_2O_3–x Dy_2O_3 were synthesized using the melt-quenching technique, and their density, molar volume, and Judd–Ofelt (JO) parameters (Ω_2, Ω_4, Ω_6) were experimentally determined. The Judd–Ofelt theory was applied to calculate spectroscopic parameters such as oscillator strengths, radiative transition probabilities, and radiative lifetimes for Dy^{3+} doped glasses. Furthermore, a Random Forest (RF) regression model was developed to predict these parameters based on the composition of the glass. The model showed high accuracy, with R^2 (Coefficient of Determination) values above 0.9 and root-mean-square errors (RMSE) under 0.1, validating the use of RF for reliable predictions of optical properties. The results indicate that the RF model can effectively simulate the luminescent properties of Rare earth (RE)-doped glasses, significantly reducing the need for experimental testing. This approach offers potential for optimizing the design of optical materials used in applications such as lasers, optical amplifiers, and temperature sensors.

1. Introduction

In the recent past, a significant amount of research effort has been performed on the investigation of luminous characteristics of lanthanide ion doped glasses. Many investigation has been directed towards the creation of infrared lasers and wide amplifiers for use in the telecommunications sector [1]. Glass networks are subject to a significant amount of impact from the local structure that is occupied by RE ions [2]. These features of the Er^{3+} ions were investigated in a variety of crystalline and non-crystalline matrices in order to investigate the possibility of using them to create lasers in the near infrared region [3][4]. Dopants have the ability to profoundly influence optical behaviour. The current investigation is making progress in the direction of the optical properties of the Er^{3+} ions. This is due to the transition from $^4I_{13/2}$ to $^4I_{15/2}$, which occurs at about 1535 nm. This transition is ideal for the optical data

∗ Corresponding author; e-mail: juginder.singh@gmail.com
https://doi.org/10.22034/crl.2024.488643.1474

transmission applications [5]. The optical gain increased up to a certain point with the concentration of Er^{3+} ions, glass network as well as the local sites along the network. In conclusion, the host matrix will eventually become optically inactive [6]. As a result of their acute and powerful emission spectra, which are caused by their 4f intra shell transitions, rare earth ions are able to function as notable luminous materials. In order to construct an effective wide band optical device that can be used in wavelength-division-multiplexing system frame works and green laser applications, it will be beneficial to utilise the green emission at around 605 nm, which corresponds to the transition from $^4I_{13/2}$ to $^4I_{15/2}$. When it comes to establishing the qualities of a glass, the composition of the base matrix is an extremely important factor. Within the last several years, there has been a substantial amount of interest in the incorporation of two or more glass modifiers into the composition for a variety of scientific and technical purposes.

Oxide glasses serve as the most robust host matrices for practical applications because to their superior chemical durability and thermal stability. Tellurite glasses, among oxide glasses, have shown significant potential as hosts for lanthanide ions, both fundamentally and in practical applications. It is well recognized that non-radiative loss is mostly governed by the highest energy phonon present in the matrix. Consequently, it is important to choose a host material with the lowest feasible maximum phonon energy. In silica, the phonon energy is rather substantial, around 1100 cm^{-1}. The vibrational frequency is quite low for chalcogenide glasses (about 300 cm^{-1}), which, yet, are deficient in certain advantageous characteristics of silica-based glasses, such as mechanical strength and chemical endurance. Tellurite glasses embody a balance between the aspiration for low phonon energy (650-750 cm^{-1}) [7-9] and the need to maintain mechanical strength and processing temperatures.

1.1 Judd-Oflet Theory

It is well known that the different spectroscopic parameters of the trivalent rare-earth ions in various hosts are calculated by the application of the theory proposed by Judd [10] and Ofelt [11]. For clarity, a brief summary of the theory is presented, taking into account only the formulas necessary to determine the different spectroscopic parameters: oscillator strengths, Judd-Ofelt parameters, radiative transition probability, branching ration and radiative lifetime. The majority of the intra configurational f-f transitions of trivalent rare earths observed in the absorption spectra are induced electric dipole transitions, although a few magnetic dipole and beyond that, it had a propensity to form a group, which altered the optical characteristics of the transitions are also present. The intensities of these transitions can be described by the oscillator strengths f_{mes} of each J-J' transition. The band absorption intensity is proportional to the oscillator strength. Experimentally it is deduced from the surface under the absorption curve. The oscillator strength f_{mes} can be calculated from the value of the absorption coefficient α(λ) at a particular wavelength λ according to the relation:

$$f_{mes} = \frac{mc^2}{\pi e^2 N} \int \frac{\alpha(\lambda) d\lambda}{\lambda^2} \quad (1)$$

Where m is the electron mass, c is the celerity of the light in the vaccum and e is the electron change. On the other side, the oscillator strength can be given in term of the electric dipole line strength S_{ed}.

$$f_{cal} = \frac{8\pi^2 mc}{3h(2J+I)\lambda} \frac{(n^2+2)}{9n} S_{ed} \quad (2)$$

$$S_{ed} = e^2 \sum_{k=2,4,6} \Omega_k |< J' | \left| U^{(k)} \right| | J > |^2 \quad (3)$$

Where $\Omega_k (k = 2,4, \text{and } 6)$ are phenomenological intensity coefficient, generally known under the name of Judd-Ofelt parameters that are dependent on both the chemical environment and the lanthanide ion [12].

The expression $(n^2+2)/9n$ considers that the rare earth ion exists in a dielectric medium rather than in a vacuum, with n being the refractive index of this medium. U(k) represents the components of the reduced tensor operator that are invariant to the ligand field. The values of U(k) are often regarded as host invariant and they are tabulated in [13]. h represents Planck's constant, whereas λ is the average wavelength of the transition. The Ω_k values are experimentally established by contrasting the estimated values derived from formula (2) with those obtained from the absorption spectra at ambient temperature of the oscillator strengths (formula (1)). When q represents the number of absorption bands analysed in experiments, resolving a system of q equations with three unknown variables by least squares approximation enables the determination of the parameters Ωk. These dimensions are articulated in cm^2.

Despite significant progress in synthesizing rare-earth doped glasses and understanding their optical properties, the traditional experimental approach to characterizing such materials can be time-consuming and resource-intensive. Each new glass composition must undergo a series of physical, chemical, and spectroscopic analyses to determine properties like the Judd–Ofelt parameters (Ω_2, Ω_4, and Ω_6), which are essential for predicting radiative transition probabilities, oscillator strengths, and other spectroscopic characteristics. These parameters are critical for designing and optimizing glass materials for

specific applications, but the manual characterization process limits the speed at which new materials can be developed.

Furthermore, the Judd–Ofelt theory itself, while robust, involves complex calculations that require precise experimental data. Although the theory provides a theoretical framework to estimate oscillator strengths and radiative properties of RE ions, its application across different glass systems is not straightforward due to variations in glass composition, structure, and local environments surrounding the RE ions. The need for an efficient and reliable method to predict these properties without the need for extensive experimental work has led to growing interest in machine learning (ML) approaches. In this paper, Random Forest (RF) are suggested to predict the spectroscopic properties of rare-earth doped glass systems, specifically the Judd–Ofelt parameters and related optical properties. RF, a subset of machine learning methods, are well-suited for modeling complex, nonlinear relationships between input variables (e.g., glass compositions) and output parameters (e.g., JO parameters).

The RF model developed in this study takes glass composition data, including the concentration of PbO, SiO_2, B_2O_3, and Dy_2O_3, as input and predicts the corresponding Judd–Ofelt parameters (Ω_2, Ω_4, and Ω_6), radiative lifetimes, and oscillator strengths as output. By training the RF on a dataset of experimentally characterized glasses, the model learns the relationship between the glass composition and its optical properties, enabling it to make accurate predictions for new glass compositions.

The remaining structure of this paper is follow as: section 2 summarized recent research on rare-earth ion-doped glasses, focusing on their structural, optical, and spectroscopic properties; section 3 describes the methodology where the glass synthesis process via the melt-quenching method and the experimental techniques used to measure density, molar volume, and spectroscopic properties; section 4 discusses the accuracy of RF predictions, supported by R^2 and RMSE metrics; section 5 discussed the conclusion of our study.

2. Review of Literature

In their study, Bayoudhi et al., (2024)[14] an undoped and Sm^{3+}-doped $45P_2O_5$–$45Na_2O$–$2Al_2O_3$–$8BaO$ glasses were synthesized using the melt-quenching method. The glass structure and luminescent characteristics were examined using Raman spectroscopy, scanning electron microscopy (SEM), spectroscopic ellipsometry, Judd-Ofelt theory, and photoluminescence. Electron microscopy demonstrated the uniformity of the samples. Raman spectroscopy demonstrated that the glass's general structure remained unaltered by Sm3+ doping, whereas ellipsometry was used to assess the optical constants. The Judd-Ofelt (JO) analysis was conducted on the absorption bands of Sm^{3+} ($4f_5$), resulting in the computation of three phenomenological parameters (Ω_2, Ω_4, and Ω_6), which were subsequently utilised to ascertain radiative properties including the radiative transition probability (Ar), the fluorescent branching ratio (βr), the stimulated emission cross-section (σe), and the radiative lifetime (τrad). The photoluminescence (PL) spectra exhibited the characteristic four transitions of Sm^{3+} at wavelengths of 564, 600, 645, and 703 nm, corresponding to the transitions $4G_{5/2} \rightarrow 6H_{5/2}$, $6H_{7/2}$, $6H_{9/2}$, and $6H_{11/2}$, respectively. The spectroscopic quality factors Ω_4/Ω_6, the projected lifespan (τrad) derived from the JO technique, and the empirically determined lifetime (τ_{exp}) for the $4G_{5/2}$ level were computed and analyzed. The glass exhibits a color purity of up to 98%, making it a viable choice for laser emission.

Bansal et al., (2024)[15] examined a novel Sm^{3+}-activated oxyfluoride glass was synthesized using the melt-quenching method followed by heat treatment. The X-ray diffraction analysis reveals the amorphous characteristics of the synthesized glasses. FTIR demonstrates that the molar excess of Bi_2O_3 enhances network connection by generating bridge oxygen sites within the structure. The Judd-Ofelt (J-O) intensity parameters demonstrate the trend $\Omega_4>\Omega_2>\Omega_6$, reflecting the stiffness of the glass structure and the ionic interaction between Sm3+ ions and adjacent ligands. The $4G_{5/2} \rightarrow 6H_{7/2}$ transition of Sm^{3+} is optimal for reddish-orange lasers because of its elevated radiative transition probability, branching ratio, and stimulated emission cross-section. The optimal emission intensity is achieved with 30 mol% Bi_2O_3, resulting in a decay time of 1.40 ms. Furthermore, the F30 glass specimen was illuminated in a reddish-orange spectrum with a correlated color temperature (CCT) of 1689 K. The thermal luminescence quenching of the synthesized glass was examined, and the activation energy for thermal stability characteristics was evaluated. The contactless optical thermometry of the glass sample was investigated within the temperature range of 303 K to 603 K using the luminescence intensity ratio (LIR) approach. The aforementioned experiments on the glass sample indicate its potential use as an active medium in lasers, non-contact optical temperature sensors, and high-energy scintillator applications.

Martinez et al., (2024)[16] stated that lithium diborate (Li_2O-$2B_2O_3$) glass, doped with Sm3+ and including silver nanoparticles, was synthesized using the melt

quenching technique. The morphological, physical, optical, and luminescent characteristics are examined. Conveyance Transmission Electron Microscopy (TEM) demonstrates the creation of silver nanoparticles, while X-Ray Diffraction (XRD) was used to confirm the amorphous nature of the vitreous phase. The UV–Vis–NIR absorption spectra demonstrated an increase of Sm3+ absorption attributable to the plasmon effect. Band gap values for all samples were determined. The emission spectra exhibited a significant transition from $4G_{5/2}$ to $6H_{7/2}$ at 603 nm when excited at 405 nm. The emission investigation verifies that luminescence increases by 2.53 times with the presence of silver nanoparticles, attributed to energy transfer between the silver nanoparticles and Sm^{3+} ions. Conventional Judd-Ofelt analysis was conducted to ascertain the J-O parameters (Ω_2, Ω_4, Ω_6). These metrics are crucial for forecasting structural behaviour and luminescent characteristics. The Judd-Ofelt findings on the generation of reddish-orange light suggest that the samples are suitable for use as laser material.

In their study, Hermann et al., (2023)[17] integrated molecular dynamics simulations, Judd-Ofelt theory, and UV–vis-NIR absorption spectroscopy to investigate the structure-sensitive hypersensitive absorption transitions of Er^{3+}, thereby enhancing the understanding of the local molecular structure surrounding doped rare earth ions as influenced by glass composition. Glasses having the compositions (35-x) BaO · x MgO · 10 Al_2O_3 · 55 SiO_2 (mol%) (x = 0, 7.5, 15, 25, 35) and (20-x) BaO · x MgO · 20 Al_2O_3 · 60 SiO_2 (mol%) (x = 0, 10, 20), doped with 2 × 10^20 ions/cm3 Er^{3+}, were synthesized and examined. Distinct variations in the absorption spectra among glasses with varying BaO/MgO ratios, reflecting differing network modifier field strengths, as well as differing ratios of network modifier oxides to Al_2O_3, are identified and examined comprehensively. Glasses characterized by elevated BaO concentrations and high ratios of network modifier oxides to Al_2O_3 exhibit reduced rare earth coordination numbers with oxygen overall, yet increased coordination probabilities with non-bridging oxygen. This phenomenon leads to significant enhancement in the splitting of optical transitions of the doped rare earth ions and heightened hypersensitivity, alongside diminished local site symmetry for the doped rare earth ions within the studied compositions. The findings, together with those from previous publications, indicate that the local symmetry of rare earth sites in glasses generally correlates with the coordination number of the rare earth elements.

Farag et al., (2023)[18] studied that the impact of Er^{3+} ions on the optical characteristics of phosphate glasses doped with a constant concentration of Sm^{3+} ions has been examined. Optical absorption analyses were conducted to determine the energy gap and Urbach energy. The Judd–Ofelt (J–O) model has been used to analyses the absorption peaks corresponding to Er^{3+} (4f11) transitions in order to ascertain the J–O intensity parameters Ωt (t = 2, 4, 6). The computed J–O parameters have been used to determine the radiative transition probabilities (Ar), branching ratios (Br), and radiative lifespan (τr) of many excited states of the Er^{3+} ion. The analysed photoluminescence spectra under UV stimulation at 380 nm exhibited many visible emission bands, hence validating the down-conversion mechanism. The energy transfer (ET) from $4S_{3/2}$ ($Er^{3+)}$ to $4G_{5/2}$ (Sm^{3+}) was confirmed. A pronounced green emission peak resulting from the $4S_{3/2} \rightarrow 4I_{15/2}$ transition was detected, exhibiting a stimulated emission cross-section of 7×10^{-21} cm².

Marzouk et al., (2023)[19] studied the lead phosphate glasses in the system [40PbO–50P_2O_5-(10-x) WO_3-xTm_2O_3], doped with varying concentrations of xTm_2O_3 ions, are prepared and subjected to a fast-cooling process. Manufactured sets exhibit significant absorption in the UV spectrum, owing to the synergistic effects of iron impurities and the involvement of Pb^{2+} ions. The presence of WO3 exhibited distinct absorption patterns attributed to the emergence of W^{5+} pentavalent ions. The physical properties of the produced glasses, including density (ρ), molar volumes (Vm), refractive index (n), optical energy gap (Eg), and Urbach energy (ΔE), were assessed. Moreover, the Judd–Ofelt coefficients for the transformation form of oscillator probabilities, fexp., fth, branching ratio, β, and radiative lifetimes, τ, of several excited states of Tm^{3+} have also been calculated. Acquire the cross-section for laser transformation stages from $3H_6$ to $3F_3$, $3H_6$ to $3H_4$, $3H_6$ to $3H_5$, and $3H_6$ to $3F_4$, together with the induced emission cross-section measured at a specified concentration of Tm_2O_3 ions in all existing glasses. Consequently, the spectroscopic properties indicate that Tm3+ doped glasses are very suitable for optical applications.

Kaur et al., (2022)[20] presented a comprehensive assessment of the structural and radiative characteristics of a series of Sm^{3+} and Gd^{3+} co-doped lead phosphate glasses with the compositions (58.2-2x) PbO - 40 P_2O_5 - 1.8 Al_2O_3 - x Sm_2O_3 - x Gd_2O_3, where x ranges from 0.4 to 1.4 mol%. The synthesized glass samples were analysed for their structural characteristics using XRD and FTIR spectroscopy. The oscillator strength of the glass samples was assessed using UV–Vis absorption spectra. The method of least squares fitting between observed and estimated oscillator strengths was used to derive Judd-Ofelt intensity parameters W_2, W_4, and W6 for elucidating the local structure and bonding characteristics around rare-earth ions. The radiative and lasing characteristics

were assessed based on intensity metrics, including the likelihood of radiative transition, branching ratio, and radiative lifetime. The emission transitions from the excited state $4G_{5/2}$ of samarium to the lower levels $6H_{5/2}$ and $6H_{7/2}$ were found to be optimal for photonic applications because of their elevated electric and magnetic dipole radiation transition probabilities, branching ratios, and stimulated emission cross sections. The glass sample PPASG4 exhibited superior radiative qualities relative to some previously documented glass configurations with comparable Sm_2O_3 concentration, indicating its potential as a contender for lasing applications.

Jose et al., (2022)[21] studied a spectroscopic study of the optical properties of the 1.06 μm ($4F_{3/2} \rightarrow 4I_{11/2}$) transition of Nd^{3+} ions at varying concentrations in fluoroborosilicate (FBSND) glasses is presented. The glass transition temperature determined by DSC research validated the thermal stability of the Nd^{3+} doped fluor borosilicate glass system. The phenomenological Judd-Ofelt parameters were assessed by applying the Judd–Ofelt (JO) theory to the observed absorption spectra and the parameters. Intense NIR emission has been detected for the lasing transition at 1.06 μm with an excitation wavelength of 584 nm. The emission intensity of all luminous bands in the NIR emission spectra of FBSND glasses increases up to 1 mol%, after which a decline in emission intensity occurs owing to concentration quenching. The significant values of JO intensity parameters and radiative characteristics, including branching ratio, stimulated emission cross section, and radiative transition probability, endorse FBSND glasses for photonic applications.

Konstantinidis et al., (2021)[22] examined the active advancement of optical materials and their applications necessitates a comprehensive knowledge of their optical characteristics, for which Judd-Ofelt (JO) theory is often used. Calculating the JO parameters ($\Omega_{2,4,6}$) required substantial experimental and theoretical effort, rendering traditional computation often impractical. To alleviate these challenges, they have examined the correlation between the JO parameters and the bulk matrix composition of a series of Er^{3+} doped tellurite glasses. The matrix compositions were used to forecast the three JO parameters by Support Vector Machine regression, in conjunction with sparse Principal Component Analysis. Initial findings indicate a robust correlation between the bulk composition and the JO parameters (root-mean-squared error ranging from 0.2053×10^{-20} to 0.5915×10^{-20}) and (mean-absolute-error varying from 0.4038×10^{-20} to 1.2291×10^{-20}), implying that with further analysis of the data and additional covariates, we may soon achieve precise characterisation of such materials with little to no experimental effort.

Basavapoornima et al., (2020)[23] focused on the spectrum analysis of Pr^{3+}:lead phosphate (PPbKANPr) glasses for applications in visible lasers and optical amplifiers, which were fabricated using a melt-cast process. The vibrational modes of PPbKANPr glasses have been examined using FTIR and Raman methods. Utilizing the absorption spectrum and the established Judd-Ofelt (JO) approach, the three JO parameters (Ω2,4,6) were computed and then used to evaluate the diverse radiative probabilities for the distinctive excited fluorescence states of Pr^{3+}. The calculated JO parameters ($\times 10^{-20}$ cm²) were $\Omega_2 = 1.51$, $\Omega_4 = 18.03$, and $\Omega_6 = 19.81$. The luminescence spectra display emission bands throughout the visible range of 480–780 nm, and when the concentration of Pr3+ ions increase, the emission intensities diminish owing to concentration quenching. The decay curves of the PPbKANPr glasses were assessed using 443 nm excitation, with monitoring conducted at the luminescence peak of 610 nm. The decay rates exhibit a bi-exponential pattern, characterised by a reduction in lifetimes as the concentration of Pr3+ ions increase. The near-infrared luminescence characteristics were elicited using the stimulation of an Ar^+ ion laser at 488 nm, resulting in a spectrum including three emission bands ranging from 800 nm to 1600 nm. The analysis of the findings demonstrated that the existing PPbKANPr glasses are effective for visible lasers and optical amplifiers.

Rao et al., (2020)[24] studied various concentrations (0.2–1.0 mol%) of Nd^{3+}-doped lead borate glass (LB) systems were synthesized by the melt quenching procedure and analysed via X-ray diffraction (XRD) and optical examinations. Three Judd-Ofelt parameters have been established from the optical absorption spectra computations. Multiple radiative factors, including radiative transition probability (A_{rad}), branching ratio (β_{cal}), absorption cross-sections (Σ), and radiative lifetime (τ_R), have been forecasted using J-O parameters. Luminescence spectra were recorded for all samples. The luminescence intensity was seen to grow progressively up to 0.8 mol % of Nd3+, after which additional concentration increments resulted in a decline in luminescence spectrum intensity. This is suggested because of the concentration quenching of neodymium ions in the LB glass matrix. The LB glass system with 0.8 mol % exhibits the highest emission intensity at 1.06 μm, corresponding to the $4F_{3/2} \rightarrow 4I_{11/2}$ transition in the near-infrared (NIR) region.

Shoaib et al., (2019)[25] shown considerable interest in luminescent glass for LED-based lighting applications.

Oxyfluoride phosphate glass samples doped with Dy_2O_3 and Eu_2O_3 were synthesised by the traditional melt quenching technique. The samples were examined by analysing their density, molar volume, refractive index, absorption spectra, emission spectra, excitation spectra, decay time profile, and by plotting their features on a CIE diagram. The density of the created glass samples was observed to increase with the quantity of ions present. The absorption spectra of glass samples created with each ions exhibited distinct absorption peaks. The excitation spectra observed for NSDy and NSEu exhibited the most pronounced peaks at 350 nm and 393 nm, respectively. It was believed that these peaks related to the transitions of $6H_{15/2}$ and $7F_0$ to the excited states $6F_{11/2}$ + $6H_{9/2}$ and $5L_6$, respectively. The Judd-Ofelt (JO) theory was used to compute the JO intensity parameters and radiative characteristics of the manufactured glass samples. The emission maxima recorded at 573 nm for NSDy and 612 nm for NSEu exhibit more intensity than the other peaks. These peaks were believed to correspond to the transitions of $6H_{13/2} \rightarrow 4F9_{/2}$ and $5D_0 \rightarrow 7F_3$, respectively. The CIE coordinates indicated that NSDy produces visible light in the white spectrum, whereas NSEu emits visible light in the reddish-orange spectrum. It was determined that both forms of glass created might serve as viable options for usage in solid-state lighting and LEDs.

3. Material & Methods

In this study, a Random Forest to predict significant physical characteristics, namely the Judd–Ofelt parameters of glass systems doped with Dy^{3+}, a rare-earth metal that enhances the luminescent qualities of these glasses. Glass compositions of 0.25 PbO–0.2 SiO_2(0.55 − x) B_2O_3–x Dy_2O_3, featuring varying Dy_2O_3 concentrations while maintaining constant PbO and SiO_2 levels, were examined. The Judd–Ofelt theory parameters, Ω_2, Ω_4, and Ω_6, together with radiative lifetimes, were delineated to examine the effects of including Dy_2O_3 into the neural network model of the glasses. Subsequently, a model using the artificial intelligence technology of Random Forest was implemented to forecast the Judd–Ofelt theory parameters, Ω_2, Ω_4, and Ω_6, together with the radiative lifetimes of the specified glass compositions and additional glass types. This approach enables the direct imitation of these critical elements while circumventing the need for costly oxide materials.

3.1 Experimental setup

- **Glasses preparation**

Glass compositions of 0.25 PbO–0.2 SiO_2–(0.55− x) B_2O_3–x Dy_2O_3 with completely different Dy_2O_3 contents and constant PbO and SiO_2 contents were prepared by the melt quenching technique. Table 1 depicts the data for each glass composition. Materials of analytical grades and 99.9% pureness B_2O_3, Dy_2O_3, PbO, and SiO_2 chemicals were used to equip the glass pieces.

Table 1. Glass compositions, density, molar volume, and concentration of Dy^{3+} of 0.25 PbO-0.2 SiO_2-(0.55-x) B_2O_3-x DY_2O_3 glasses.

Samples	Composition mol%				Density (g.cm-3)	Molar Volume (cm3/mol)	Vtx10^{-6} (cm3/mol)
	PbO	SiO_2	B_2O_3	Dy_2O_3			
S1	24	21	56	0	3.822	27.76	0.796
S2	24	21	55	1	3.869	28.21	0.776
S3	24	21	53	3	3.964	29.07	0.739
S4	24	21	52	5	4.058	29.88	0.704

Appropriate amounts of each powder type were measured using a digital balance (HR-200) with a sensitivity of ±0.0001 g. The chemical mixture's uniformity was attained by continual grinding with agate mortar. The combination was heated to 727 K for 60 minutes to eliminate water vapour and CO_2, resulting in a bubble-free liquid. The mixture was blended intermittently to achieve uniformity. Upon achieving the requisite consistency, the melt was cast into a stainless-steel mould and then subjected to a furnace treatment at 573 K for two hours to alleviate mechanical tensions. Bulk samples of glass measuring 1 × 1 × 4 cm^3 were subsequently acquired.
Each glass sample was polished on a glass plate using fine aluminum oxide abrasive and machine oil. A variance of around ±20 µm was observed in the sample thickness. The amorphous nature of glasses was highlighted using X-ray diffraction (XRD). The absorption spectra of Dy^{3+}-doped samples were recorded using a JAS-CO V-570 dual-beam photometer within the 200–3000 nm range at ambient temperature. In the UV/VIS spectrum, the resolution was ±0.3 nm, but in the NIR range, the resolution was ±1.6 nm.

- **Density Measurements**

The density (ρ) of glasses was determined by using the Archimedes principle with toluene, which was used as the buoyant gas, and the connection as follows:

$$\rho = \rho_x \left(\frac{W_a}{W_a - W_x}\right) \quad (4)$$

Where ρ_x is the density of toluene, Wa and Wx are the weights of the sample in the air and in toluene, respectively. We repeated the experiment 3 times and the error was $\pm \frac{0.005g}{cm^3}$.

- **Judd-Ofelt Analysis**

The Judd–Ofelt theory [26][27] was used to calculate the transition probabilities of Dy3+ excited states. The computed oscillator strength for each transition is:

$$f_{cal}[(S,L)J;(S',L')J'] = \frac{8\pi^2 mc}{3h\lambda(2J+1)} \times \frac{(n^2+2)^2}{9n} \times \sum_{\lambda=2,4,6} \Omega_\lambda | < (S,L)J > \left|\left|U^\lambda\right|\right| < (S',L')J'|^2 \quad (5)$$

Where m, h, c, n, λ and $< \left|\left|U^\lambda\right|\right| >$, are the electronic mass, planck's constant, the speed of light, the host-glass index of refraction, the mean transition wavelength, and the double reduced matrix components of the unit tensor obtained from Weber [28]. Radial integrals, denominator of perturbations, and odd-dispute expressions of crystalline domain are all parameters of the Judd-Ofelt theory $\Omega_{2,4,6}$.

The simulated strengths of the oscillator, defined as the f-exp of transitions, may be determined by integrating each absorption band as seen in Figure 1, according to the equation:

$$f_{exp} = 2.303 \frac{mc^2}{iN\pi e^2} \int \frac{OD(\lambda) d\lambda}{d\lambda^2} \quad (6)$$

The electron charge, specimen thickness, active ion density number, and optical density are denoted by the parameters e, l, N, and $OD(\lambda)$, respectively. The Judd–Ofelt theory parameters, including Ω_2, Ω_4, and Ω_6 were computed using the least-squares matching methods as stipulated by the Judd–Ofelt theory. The match fineness is determined by the variance of the root mean square (RMS), which is established by:

$$r.m.s = \left[\sum_P \frac{(f_{calc} - f_{meas})^2}{P-3}\right]^{1/2} \quad (7)$$

Where is the P number of different types of focused attention transition throughout the spectrum. The following equations will be used to sample the Judd-Ofelt Ω_2, Ω_4, and Ω_6 parameters in order to obtained the transition radiative possibilities for dipole transitions between excited states, and thus the minimum lie level of Dy^{3+}.

$$A(k,k') = \frac{64\pi^2 e^2}{3h\lambda^3(2k+1)} \times \frac{n(n^2+2)^2}{9} \times \sum_{\lambda=2,4,6} \Omega_\lambda | < (S,L)k > \left|\left|U^\lambda\right|\right| < (S',L')k' > |^2 \quad (8)$$

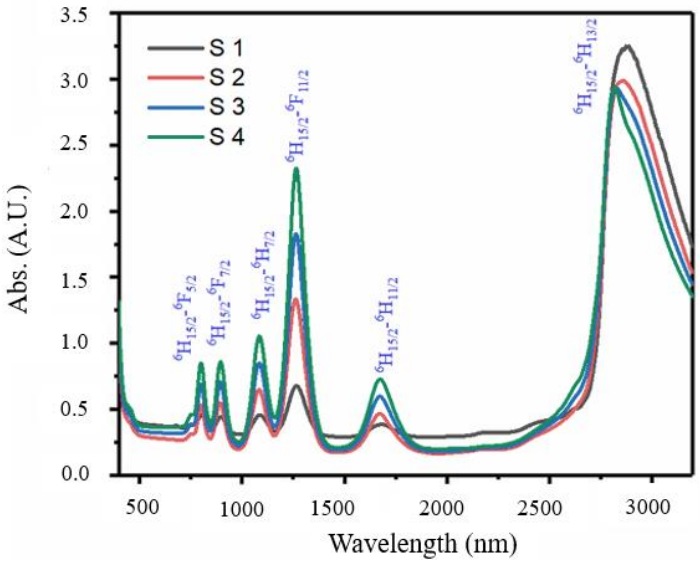

Fig. 1. Absorption spectra of glass composition (S1-S4) with their transitions.

The converse of the sum of A (k, k') values calculated via terminal levels is used to ascertain the radiative lifetimes of the associated stimulated energy levels:

$$\tau_{rad} = \frac{1}{\sum A(k,k')} \quad (9)$$

The radiative lifetimes were delineated for all potential transitions from the upper J-manifolds $6H_{13/2}$, $6H_{11/2}$, $6F_{11/2}$, $6H_{7/2}$, $6F_{7/2}$, and $6F_{5/2}$ to all minimal lying states of Dy^{3+} in the host glass.

- **RF-Regression model**

Random Forest-Regression is an ensemble learning method that operates by constructing multiple decision trees at training time and outputting the mean of the predictions from these individual trees. It is based on the principle that multiple weak learners (decision trees) combined together form a strong learner, reducing overfitting and improving the model's generalization ability.

This paper used an RF to forecast critical parameters, including Ω_2, Ω_4, Ω_6, and radiative lifetimes, to optimize cost and time efficiency. Conversely, the RF is constrained by the availability of a small data subset for network creation and training; it is susceptible to data accuracy, which often influences the precision of the predictions. This indicates that if the training data is erroneous, the projected outcomes will also be erroneous, not due to the methodology but rather due to the accuracy

of the information. In the RF-regressor architecture, the input layer functions as a signal distributor, while the hidden layers serve as signal receptors. The output layer functions as a collector of detected features and a source of responses. Every output neurone is connected to its inputs (Xi). The outputs (Yj) of the jth neurones in a layer are defined by two equations as follows:

$$U_j = \sum(X_i w_{ij}) \qquad (10)$$

And

$$Y_j = F_{th}(U_j + t_j) \qquad (11)$$

This study employs the hyperbolic function, transforming it into a sigmoid function by a mathematical equation (see to Equation (11)). This is due to the hyperbolic function being seen as a switch inside the media domain, since it is distinguished by its smoothness. The significance of suppression approaching zero is paramount owing to its range of 1 to +1, in contrast to the sigmoid function's range of 0 to 1, although values will become elevated upon attaining the maximum level.

$$f(x) = \frac{1}{1+e^{-x}} \qquad (12)$$

The final output (Yj) serves as either an input for the subsequent layer or a constraint for the neural architecture if it is the terminal layer. The training phase is the second stage in the neural network process. The objective of this operation is to calibrate the neural network until it generates an output. The error is computed by contrasting the anticipated output with the actual output and is then transmitted back through the network.

The procedure is repeated for several rounds until the discrepancies between the intended and actual output are minimized to the specified tolerance. Once the neural network eliminates every error and attains the specified tolerance, the training process may cease. The inaccuracy disseminates in the neural network beginning at the output layer as follows:

$$wij = w'_{ij} + LR(e_j Xi) \qquad (13)$$

And

$$e_j = Y_j(1 - Y_j)(d_j - Y_j) \qquad (14)$$

Where wij is the corrected weight, w'_{ij} is the prior worth of the weight, LR is the rate of learning, e_j is the error code, Xi is the ith value of the input, Y_j is the output, and d_j is the desirable output.

A computational model using RF techniques was developed to replicate and forecast the Judd–Ofelt parameters of several glasses, including Ω_2, Ω_4, and Ω_6 as well as their radiative lifetimes. To develop a neural network model, it is essential to define the initial input and output variables. Table 2 delineates the main input and output variables of the neural network; T denotes the input variable and 'O' represent the output variable.

Table 2. Additional key input variables and output variables for all the RF models.

Models	RF1	RF2	RF3	RF4
SiO_2	I	I	I	I
Dy_2O_3	I	I	I	I
B_2O_3	I	I	I	I
BaO	I	I	I	I
LiF	I	I	I	I
NaF	I	I	I	I
PbO	I	I	I	I
P_2O_5	I	I	I	I
S2	O	-	-	-
S4	-	O	-	-
S6	-	-	O	-
T	-	-	-	O

2.4 Data Splitting and Performance Metrics

To assess machine-learning models, the data were partitioned into training and validation sets to ensure that predictions were made using distinct data records not used in the model's training. This research included training the learning model on 75% of the input data and validating it on the remaining 25%. Various performance measures exist to assess the loss in forecasting models, including R squared (R^2) and root-mean-square error (RMSE). The R^2 quantifies the degree to which the forecasting model accounts for the variability of the results. Equation (15) delineates the computation of R squared. The second metric, RMSE, quantifies the discrepancies between actual and projected values, computed as outlined in Equation (16), where $M, y_j, \hat{y}_j, and\ \bar{y}$ represent the number of samples, actual values, forecasted values, and the mean of the actual values, respectively.

$$R^2 = 1 - \frac{\sum_{j=1}^{M}(yi-\hat{y}_j)^2}{\sum_{j=1}^{M}(yi-\bar{y})^2} \quad (15)$$

$$RMSE = \sqrt{\frac{1}{M}\sum_{J=1}^{M}(y_i - \hat{y}_j)^2} \quad (16)$$

4. Result and discussion

4.1 Density and Molar Volume

Figure 4 displays the change in density after supplementation with various Dy_2O_3 mol percentages at the expense of B_2O_3. The density values were found to increase as the Dy_2O_3mol percent increases. If we consider the additive rule of density, we can expect a rise in density values with the addition of Dy_2O_3. Dy_2O_3 has a density of 7.80 g/cm^3, which is significantly higher than B_2O_3 (2.55 g/cm^3) [29]. It is known that the structural unit of B_2O_3-based glasses gradually varies from BO_4 units to BO_3 with the rising the quantities of other components.

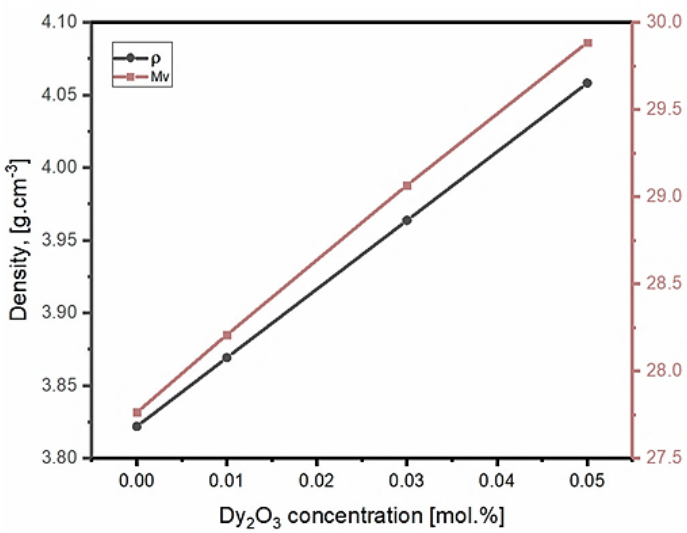

Fig. 4. Variation of density and molar volume with the Dy_2O_3 concentration.

Similarly, molar volume (Vm) was found to increase with rising Dy_2O_3 content as seen in Figure 4. This rise was anticipated because the atomic radii of dysprosium and boron atoms are 1.75 Å and 0.85 Å, respectively. Generally, the rise in molar volume points to the increase in spaces in the lattice framework of the glass. Therefore, the rise in molar volume with rising Dy_2O_3 content emphasizes the transference of BO_3 units from BO_4 units with oxygen atoms that are non-bridging, and thus means the framework becomes significantly more open.

4.2 Judd-Oflet Analysis of Dy^{3+} Intensity

The estimated and experimentally specified oscillator strength for Dy^{3+} in PbO-SiO_2-B_2O_3 glasses were recorded at room temperature as displayed in Table 3. The values of experimentally specified f_{exp} and computed f_{cal} oscillator strength is higher for $6H15/2 \rightarrow 6H13/2$ transition in every glass lattice. The fineness among the experimental and computed oscillator strengths grained by root means square (RMS) drifts. It is pointed attention that, for $\frac{6H15}{2} \rightarrow \frac{6H13}{2}, \frac{6H15}{2} \rightarrow \frac{6H11}{2}, \frac{6H15}{2} \rightarrow \frac{6F13}{2}, \frac{6H15}{2} \rightarrow \frac{6H7}{2}, \frac{6H15}{2} \rightarrow \frac{6f7}{2}, and\ 6H15/2 \rightarrow \frac{6f5}{2}$ transitions, the experimental oscillator stresses are in productive sensible consent with the computed values, pointing the legality of using the theory of Judd-Ofelt computations on the glass compositions.

Table 3. Experimental f_{exp} and calculated f_{cal} oscillator strengths along (from the ground state, $6H1_{5/2}$), with JO parameters of prepared glass samples.

Transition 6H15/2	Wavelength nm	Energy (cm^{-1})	S2		S3		S4	
			f_{exp}	f_{cal}	f_{exp}	f_{cal}	f_{exp}	f_{cal}
6H13/2	2852	3506	-	-	5.78	4.832	2.943	2.986
6H11/2	1714	5834	1.623	1.710	1.746	1.840	1.750	1.852
6F11/2	1293	7733	5.78	5.47	5.78	5.722	5.802	5.756
6H7/2	1097	9115	-	-	2.188	2.077	2.703	2.07
6F7/2	907	11025	1.76	1.784	1.522	1.544	1.520	1.522
6F5/2	804	12437	0.822	0.724	0.6244	0.609	0.604	0.587
Ω_2 10-20 cm^2	-	-	3.632	-	5.124	-	5.378	-
Ω_4 10-20 cm^2	-	-	2.692	-	0.888	-	0.626	-
Ω_6 10-20 cm^2	-	-	1.932	-	1.934	-	2.056	-
RMS	-	-	0.320	-	0.281	-	0.201	-

Table 3 indicate the parameters gained from the Judd-Ofelt theory, including Ω_2, Ω_4 and Ω_6. Ω_2 is linked to the host-glass dispute, although Ω_6 decrease as the covalence quality of the Dy-O bonds improves. A distinctive merit of the Ω_2 parameter is linked to the non-symmetry of the framework coordinates. The ligand polarizability of the molecular or ions, as well as the quality of bonding, is sensitive to the local circumference of the RE ions. The other two Judd-Ofelt theoretical parameters, Ω_4 and Ω_6, include qualities such as the viscosity and hardness of the glass framework and dielectric media that inspire bonding between ligand atoms, as well as dysprosium ions.

The radiative lifetime was specified for all the probable transitions from superior J-manifolds $6H1_{3/2}$, 6H11/2, 6F11/2, 6H7/2, 6F7/2, and 6F5/2 to all minimum lie states of the Dy^{3+} in the borate host glass. The radiative lifetime for the $6H_{13/2}$ state in glasses S2, S3, and S4 were 72.56, 77.42 and 74.83ms, respectively as displayed in Table 4.

Table 4. Calculated lifetime (τ, ms) of glass samples.

Transition $^6H_{15/2}$	**S2**	**S3**	**S4**
	τ(ms)	**τ (ms)**	**τ (ms)**
$^6H_{13/2}$	72.56	77.42	74.83
$^6H_{11/2}$	15.82	14.03	13.33
$^6F_{11/2}$	1.64	1.55	1.49
$^6H_{7/2}$	17.20	17.84	17.48
$^6F_{7/2}$	0.16	0.19	0.19
$^6F_{5/2}$	0.78	0.84	0.92

The model that exploited the RF as an exercise model was resolved to be used for predicting the density, the parameters of Judd–Ofelt theory, Ω_2, Ω_4 and Ω_6, and the radiative lifetimes of our inspected glass compositions. Over 35 glass compositions were used in the learning model. The benefit of our model is that it allowed for the explicit mimicking of significant features of glasses without melting the raw oxide materials, relying on a number of theoretical parameters such as molar weights and oxide densities as inputs to the model to produce the expected outputs.

The outcomes of the R^2 and RMSE and mean absolute error (MAE) calculations for the RF regression model on the validation data records are shown in Table 5. The use of the PCA as a preprocessing step for the input variables is compromised as a consequence of the anticipated values for the outputs. Despite this, the PCA produced accuracy that was lower than expected, as seen by the results of the R^2 and RMSE and MAE. Consequently, this performance is returned as it obtains the linear latent feature in the feature space.

Table 5. RMSE and R^2 of the RF predicting models

Outcome	**T**	**T(PCA)**	**S2**	**S2 (PCA)**	**S4**	**S4 (PCA)**	**S6**	**S6 (PCA)**
RMSE	0.070	0.007	0.106	0.158	0.062	0.104	0.062	0.082
R^2	0.938	0.923	0.912	0.868	0.932	0.844	0.942	0.928
MAE	0.107	0.010	0.182	0.247	0.092	0.168	0.095	0.124

Figures 5-7 display the variations of the experimentally gained values of density, molar volume, parameters of the Judd-Ofelt theory Ω_2, Ω_4, and Ω_6, and radiative lifetimes with those that were predicted utilizing the resolved model in this work. The linear- regression process was utilized to display the agreement between the experimentally measured values and the values predicted using RF. Solid straight lines display slopes that are within the unity domain, confirming the agreement between the experimental and predicted results. Every figure displays the slopes and correlation factors. Taking into account the uncertainties of the experimental data, the agreements in Figure 6 were very satisfactory. In all cases, the difference between the forecasted and experimentally obtained values was less than 0.5%, and in the inspected glasses, it was less than 5%. The proposed methodology can be a good alternative for problems in astrophysics, plasma physics, atomic physics, thermodynamics, electromagnetics, machines, nanotechnology, fluid mechanics, electrohydrodynamic, signal processing, power, energy, bioinformatics, economics and finance.

The productive and sensitive approach for predicting our results shows that the resolved RF model is a good tool for the simulation of the luminescence properties of rare-earth-doped glasses and can consequently lead to saving money from grants.

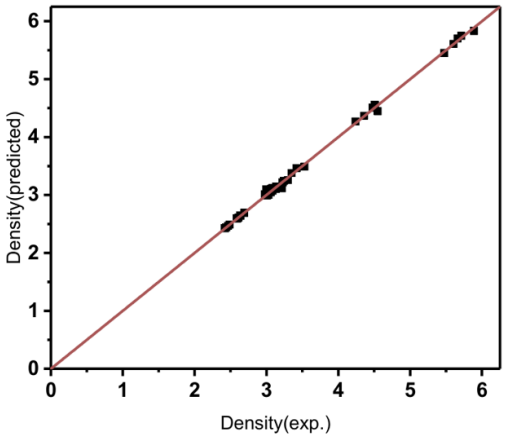

Fig. 5. Experimentally measure density against predicted density using RF.

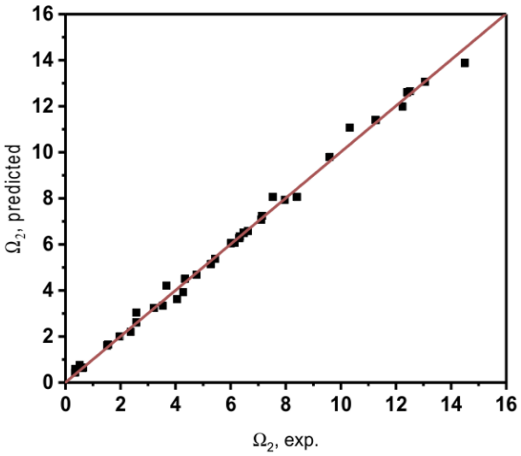

(a)

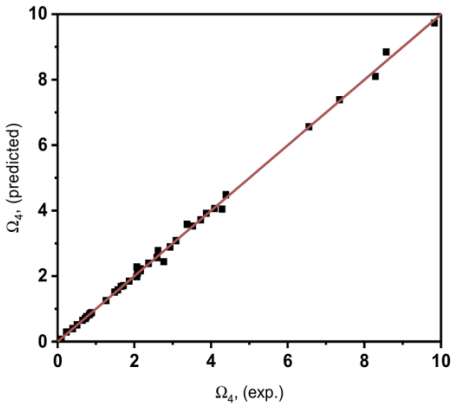

(b)

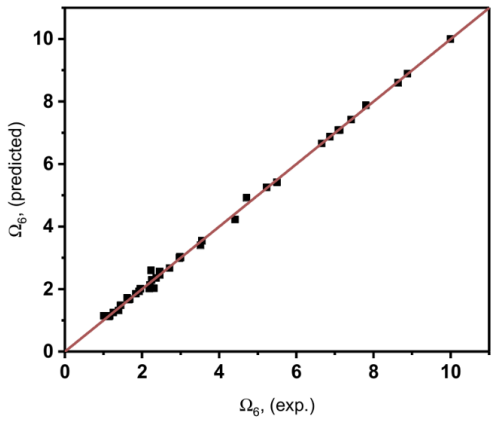

(c)

Fig. 6. Experimentally calculated Judd-Ofelt parameters compared against predictions generated by RF. (a) Estimated Judd-Ofelt parameters Ω_2 using RF. (b) Estimated Judd-Ofelt parameter Ω_4 compared to anticipated Ω4 using RF. (c) Estimated Judd-Ofelt parameter Ω_6 compared to anticipated Ω_6 using RF.

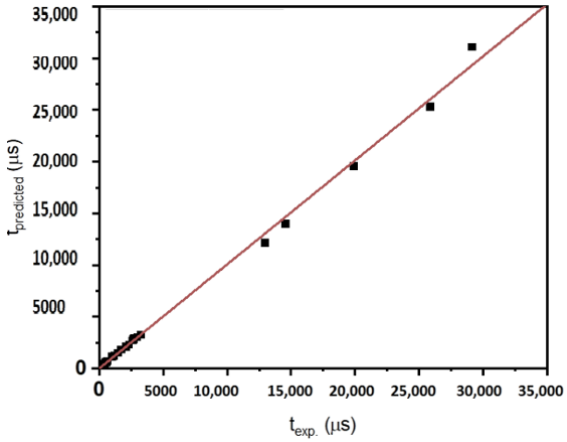

Fig. 7. Experimentally estimated lifetime t against predicted utilizing RF.

The efficacy of the findings in this study using RF-regression models was juxtaposed with previous ML-based research, including the works of Ahmmad [30], BENHADJIR [31], and Ahmed et al. [32]. In [30], two machine learning methods. The k-nearest neighbour (KNN), and artificial neural network (ANN) were used in predicting glass density. The R2 result was 0.62, in contrast to 0.975 in our analysis. In [31], the Judd–Ofelt parameters (Ω_2, Ω_4, and Ω_6) were determined via the ANN approach. The obtained RMSE values for the retrieved results of Ω_2, Ω_4, and Ω_6 were 1.4843, 0.5938, and 0.5136, respectively, in contrast to 0.106, 0.062, and 0.062 in this investigation.

5. Conclusion

The density, Judd–Ofelt parameters Ω_2, Ω_4, and Ω_6, and radiative lifetimes of oxide glasses were evaluated using the RF model. There was a significant concordance between the measured and predicted values for more than 35 unique borate and silicate glasses. The concentrations of rare-earth ions, glass densities, molecular weights, and molar volumes served as inputs, while the outputs were the corresponding Judd–Ofelt parameters. We used the resolved model to formulate a novel glass composition of 0.25 PbO–0.2 SiO_2–(0.55– x) B_2O_3–x Dy_2O_3. The finalized model shown a unique ability to ascertain the glass frameworks before doing the testing activity. The experimental findings of the Judd–Ofelt parameters for the glass system indicated a reduction in the covalence quality of the bonds. The reduction in the bond's covalent character correlates well with the decline in packing density, Vt. Consequently, Dy^{3+} ions have been regarded as prospective luminous centres.

Disclosure statement

The authors declare no conflict of interest.

Data Availability Statement

The datasets used and/or analyzed during the current study are available from the corresponding author on reasonable request.

References

[1] D. Murthy, T. Sasikala, B. Jamalaiah, A.M. Babu, J.S. Kumar, M. Jayasimhadri, L.R. Moorthy, Investigation on luminescence properties of Nd3+ ions in alkaline-earth titanium phosphate glasses, Optics communications 284 (2011) 603-607.

[2] D.E. Day, Mixed alkali glasses—their properties and uses, Journal of Non-Crystalline Solids 21 (1976) 343-372.

[3] S. Tanabe, Optical properties and local structure of rare-earth-doped amplifier for broadband telecommunication, Journal of alloys and compounds 408 (2006) 675-679.

[4] D.K. Sardar, C.C. Russell III, R.M. Yow, J.B. Gruber, B. Zandi, E.P. Kokanyan, Spectroscopic analysis of the Er 3+(4f 11) absorption intensities in NaBi (WO 4) 2, Journal of applied physics 95 (2004) 1180-1184.

[5] K. Selvaraju, K. Marimuthu, Structural and spectroscopic studies on concentration dependent Sm3+ doped boro-tellurite glasses, Journal of Alloys and Compounds 553 (2013) 273-281.

[6] A. Kenyon, Recent developments in rare-earth doped materials for optoelectronics, Progress in Quantum electronics 26 (2002) 225-284.

[7] A. Hishikawa, H. Hasegawa, K. Yamanouchi, Hydrogen migration in acetonitrile in intense laser fields in competition with two-body Coulomb explosion, Journal of electron spectroscopy and related phenomena 141 (2004) 195-200.

[8] C. Joshi, R. Rai, S. Rai, Structural, thermal, and optical properties of Er3+/Yb3+ co-doped oxyhalide tellurite glasses, glass-ceramics and ceramics, Journal of Quantitative Spectroscopy and Radiative Transfer 113 (2012) 397-404.

[9] M.C. Gonçalves, L.F. Santos, R.M. Almeida, Rare-earth-doped transparent glass ceramics, Comptes rendus. Chimie 5 (2002) 845-854.

[10] B.R. Judd, Optical absorption intensities of rare-earth ions, Physical review 127 (1962) 750.

[11] G. Ofelt, Intensities of crystal spectra of rare-earth ions, The journal of chemical physics 37 (1962) 511-520.

[12] G. De Sa, O. Malta, C. de Mello Donegá, A. Simas, R. Longo, P. Santa-Cruz, E. da Silva Jr, Spectroscopic properties and design of highly luminescent lanthanide coordination complexes, Coordination Chemistry Reviews 196 (2000) 165-195.

[13] W. Carnall, P. Fields, K. Rajnak, Electronic energy levels in the trivalent lanthanide aquo ions. I. Pr3+, Nd3+, Pm3+, Sm3+, Dy3+, Ho3+, Er3+, and Tm3+, The Journal of chemical physics 49 (1968) 4424-4442.

[14] D. Bayoudhi, C. Bouzidi, E. Matei, M. Secu, A.C. Galca, Optical characterization of Sm3+ doped phosphate glasses for potential orange laser applications, Journal of Luminescence 265 (2024) 120204.

[15] K. Bansal, N.K. Mishra, I. Abdullahi, P.J. Singh, M. Tyagi, S. Singh, Studies of luminescence traits and Judd-Ofelt analysis of Sm3+ activated oxyfluoride glasses, Optical Materials 147 (2024) 114579.

[16] J.L.C. Martínez, L.A. Diaz-Torres, J.A. Elias, T.G. Alaniz, A. Torres-Castro, M. Vallejo, Laser parameters analysis of Li2O-2B2O3 glass doped with Sm3+ and containing Ag nanoparticles, Optical Materials 154 (2024) 115788.

[17] A. Herrmann, A. Assadi, R. Lachheb, M. Zekri, A. Erlebach, K. Damak, R. Maâlej, M. Sierka, C. Rüssel, The effect of glass structure and local rare earth site symmetry on the optical properties of rare earth doped alkaline earth aluminosilicate glasses, Acta Materialia 249 (2023) 118811.

[18] M. Farag, A. Elbakey, M. El-Mansy, T. Elrasasi, Judd–Ofelt and spectroscopic analysis of erbium ions co-doped with samarium ions in phosphate glasses environment, Optical and Quantum Electronics 55 (2023) 358.

[19] S.Y. Marzouk, A.Y. Sayed, Linear, non-linear refractive index and Judd-Ofelt parameters of Tm2O3-doped P2O5-PbO-WO3 glasses, Optical Materials 135 (2023) 113377.

[20] P. Kaur, D. Kaur, D. Singh, M. Al-Buriahi, A. Al-Baradi, T. Singh, Detailed spectral evaluation of rare earth co-doped glasses for photonic applications, Journal of Luminescence 246 (2022) 118861.

[21] A. Jose, T. Krishnapriya, J.R. Jose, C. Joseph, P. Biju, NIR photoluminescent characteristics of Nd3+ activated fluoroborosilicate glasses for laser material applications, Physica B: Condensed Matter 634 (2022) 413772.

[22] M. Konstantinidis, E. Lalla, G. Lopez-Reyes, U. Rodríguez-Mendoza, E. Lymer, J. Freemantle, M. Daly, Statistical learning for the estimation of Judd-Ofelt

parameters: A case study of Er3+: Doped tellurite glasses, Journal of Luminescence 235 (2021) 118020.
[23] C. Basavapoornima, C. Kesavulu, T. Maheswari, W. Pecharapa, S.R. Depuru, C. Jayasankar, Spectral characteristics of Pr3+-doped lead based phosphate glasses for optical display device applications, Journal of Luminescence 228 (2020) 117585.
[24] K.V. Rao, S. Babu, C. Balanarayana, Y. Ratnakaram, Comparative impact of Nd3+ ion doping concentration on near-infrared laser emission in lead borate glassy materials, Optik 202 (2020) 163562.
[25] M. Shoaib, N. Chanthima, G. Rooh, R. Rajaramakrishna, J. Kaewkhao, Physical and luminescence properties of rare earth doped phosphate glasses for solid state lighting applications, Interdisciplinary Research Review 14 (2019) 20-26.
[26] B.R. Judd, Optical absorption intensities of rare-earth ions, Physical review 127 (1962) 750.
[27] G. Ofelt, Intensities of crystal spectra of rare-earth ions, The journal of chemical physics 37 (1962) 511-520.
[28] W.F. Krupke, J.B. Gruber, Optical-absorption intensities of rare-earth ions in crystals: the absorption spectrum of thulium ethyl sulfate, Physical Review 139 (1965) A2008.
[29] M. Weber, Spontaneous emission probabilities and quantum efficiencies for excited states of Pr3+ in LaF3, The Journal of Chemical Physics 48 (1968) 4774-4780.
[30] D.R. Lide, CRC handbook of chemistry and physics, CRC press2004.
[31] A. BENHADJIR, Judd-Ofelt parameters: Bayesian inference and deep learning approach, 2021.
[32] S.A. Ahmed, S. Rajiya, M. Samee, S.K. Ahmmad, K.A. Jaleeli, Density of bismuth boro zinc glasses using machine learning techniques, Journal of Inorganic and Organometallic Polymers and Materials 32 (2022) 941-953.